Electronically Coupled Nanocrystal Superlattice Films by *in Situ* Ligand Exchange at the Liquid–Air Interface

Angang Dong,*,†,§ Yucong Jiao,‡ and Delia J. Milliron§,⊥

†Department of Chemistry and ‡Department of Macromolecular Science, Fudan University, Shanghai 200433, P. R. China, §The Molecular Foundry, Lawrence Berkeley National Laboratory, Berkeley, California 94720, United States, and ⊥Department of Chemical Engineering, The University of Texas at Austin, Austin, Texas 78712, United States

ABSTRACT The ability to remove long, insulating ligands from nanocrystal (NC) surfaces without deteriorating the structural integrity of NC films is critical to realizing their electronic and optoelectronic applications. Here we report a nondestructive ligand-exchange approach based on *in situ* chemical treatment of NCs floating at the liquid–air interface, enabling strongly coupled NC superlattice films that can be directly transferred to arbitrary substrates for device applications. Ligand-exchange-induced structural defects such as cracks and degraded NC ordering that are commonly observed using previous methods are largely prevented by performing ligand exchange at the liquid–air interface. The significantly reduced interparticle spacing arising from ligand replacement leads to highly conductive NC superlattice films, the electrical conductivities and carrier mobilities of which are 1 order of magnitude higher than those of the same NC films subject to substrate-supported exchange using previously reported procedures. The *in situ*, free-floating exchange approach presented here opens the door for electronically coupled NC superlattices that hold great promise for high-performance, flexible electronic and optoelectronic devices.

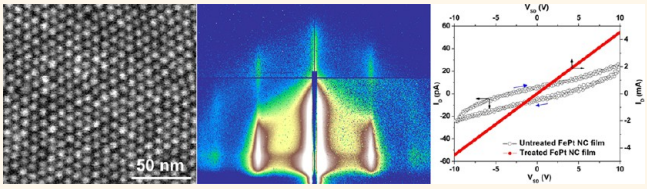

KEYWORDS: nanocrystal superlattices · ligand exchange · electronic coupling · *in situ* treatment · nanocrystal devices · liquid–air interface

Thin films of self-assembled nanocrystal (NC) superlattices have emerged as prospective granular materials for electronic and optoelectronic devices,[1−12] primarily due to collective properties arising from coupling interactions of constituent NCs.[13−15] However, as-formed NC superlattices are only weakly coupled as a result of large interparticle spacing maintained by long-chain insulating ligands at NC surfaces.[5] To facilitate charge transport through NC films, post treatment is required to reduce interparticle spacing to enhance electronic coupling between NCs, typically by replacing the native long ligands with shorter ones.[16−31] Many current approaches rely on a substrate-supported exchange strategy, in which NC films deposited on a substrate are dipped in a solution containing short ligands for chemical treatment.[16−25] Although electrically conductive NC films can be obtained by this approach, severe film cracking caused by the lost volume is commonly observed.[16−19] Deposition of additional NCs followed by exchange is required to fill cracks and obtain continuous films, which will inevitably lead to the degradation of long-range NC ordering.[16] Such structural defects can drastically influence charge transport characteristics of NC films and are therefore undesirable for device applications.[23] Alternatively, NCs can also be treated by *ex situ* exchange in solvent dispersions, and conductive films are accessible by spin-coating or drop-casting the solution-exchanged NCs.[24−31] Despite the possibility to avoid cracks by this approach, disordered NC films typically result due to the surface modification of NCs,[25] with the exception of Au NCs which have been reported to form superlattice films after exchange with chalcogenidometallates or metal chalcogenide complexes (MCCs).[27] Furthermore, many recently applied short ligands such as hydrazine,[16] 1,2-ethanedithiol (EDT),[17] and formic acid[21] are not appropriate for solution exchange, as NCs treated by such ligands are no longer dispersible for solution processing. Therefore, it still remains a challenge

* Address correspondence to agdong@fudan.edu.cn.

Received for review September 1, 2013 and accepted November 19, 2013.

Published online November 19, 2013
10.1021/nn404566b

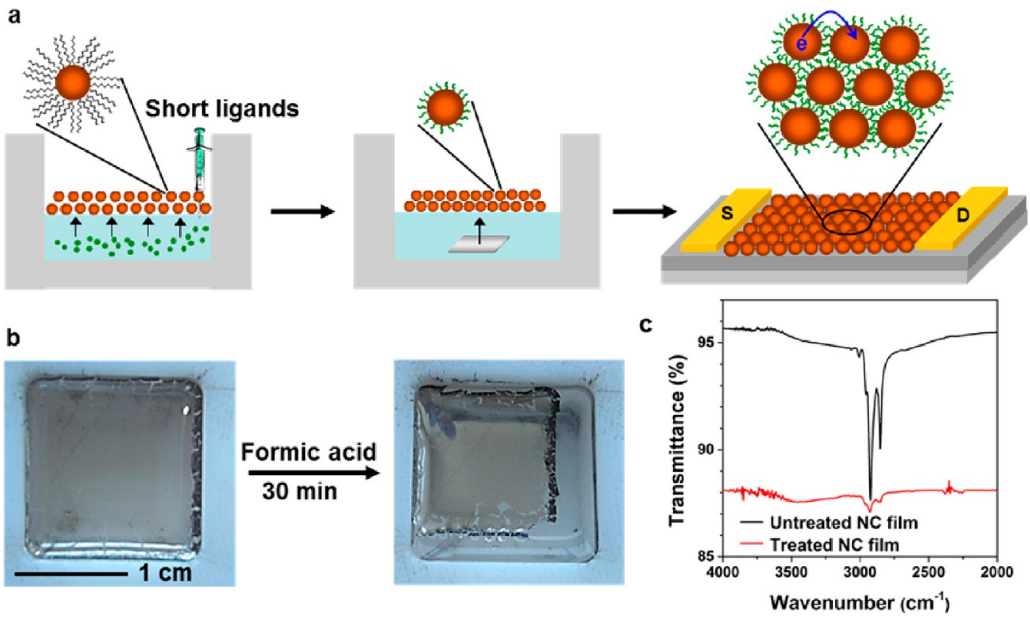

Figure 1. (a) Schematic illustration of *in situ* ligand exchange at the liquid−air interface. (b) Photographs of an FePt NC superlattice monolayer subject to free-floating exchange with formic acid, showing the macroscopic film contraction. The cracks in the bottom right corner of the treated NC film are caused by the inserted syringe. (c) FTIR spectra of FePt NC films before and after formic acid treatment, respectively; absolute transmittance spectra have been offset for clarity.

to form crack-free, electronically coupled NC superlattice films.

In this work, we report that strongly coupled, geometrically ordered NC films over large areas (~1 cm^2) can be obtained by *in situ*, free-floating exchange of NC superlattices preassembled at the liquid−air interface. Different from previous substrate-supported exchange approaches,[16−20] performing surface treatment of NC films on a liquid surface allows macroscopic film contraction with ligand removal, thereby largely preventing crack formation while preserving the local NC ordering. The resulting NC superlattice films are highly conductive, with an electrical conductivity and carrier mobility 1 order of magnitude greater than those of the same NC films subject to substrate-supported exchange. In addition, both self-assembly and ligand-exchange processes proceed at the liquid−air interface, enabling ready integration of conductive NC films onto arbitrary substrates for device fabrication. This approach is applicable to different NCs and compatible with a variety of short ligands, paving the way toward electronically coupled NC superlattices that are highly desirable for high-performance, flexible electronic and optoelectronic devices.[7,31−33]

RESULTS AND DISCUSSION

The free-floating exchange strategy is proposed by taking advantage of the liquid−air interfacial assembly approach we have recently developed for the growth of large-area, transferrable NC superlattice films.[6,34] As schematically illustrated in Figure 1a, controlled drying of NC solution in hexane on the surface of acetonitrile confined in a Teflon well yields a floating NC superlattice film, the thickness of which is tunable from monolayers to multilayers by varying NC concentration. After the NC film formation, an acetonitrile solution containing the chosen short ligands is injected into the subphase *via* a syringe for ligand exchange (see Methods). The resulting surface-treated NC film can be readily transferred from the liquid surface to any substrate for characterization and device fabrication. We note that the heat treatment of NC superlattice films floating on an immiscible liquid surface has been recently studied by Vanmaekelbergh *et al.*,[12] and they found that 1D and 2D nanostructured sheets could be formed *via* oriented attachment of PbSe NCs by controlling NC concentration and temperature. To the best of our knowledge, chemical treatment of floating NCs using various short ligands to form electronically coupled superlattice films has not been reported to date.

Figure 1b shows photographs of a floating superlattice film self-assembled from 6.0 nm oleic-acid-capped FePt NCs.[35] Notably, the film area is reduced by ~40% after *in situ* ligand exchange with formic acid for 30 min, whereas the film's integrity is retained without macroscopic cracking or crumpling. The dramatically decreased C−H stretch absorption band in Fourier transform infrared (FTIR) spectra indicates that the majority of oleate is removed by formic acid treatment (Figure 1c).[21]

The film microstructures are characterized by transmission electron microscopy (TEM) and high-resolution scanning electron microscopy (HRSEM), which reveal a well-preserved NC superlattice structure upon formic acid treatment, despite the significantly reduced interparticle spacing (Figure 2a−c). In sharp contrast, a cracked film without any NC ordering results when the pristine NC superlattice film is transferred to a Si wafer

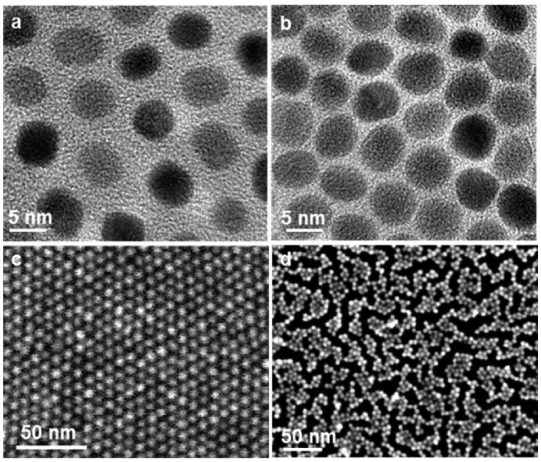

Figure 2. (a, b) TEM images of FePt NC superlattice monolayers before and after free-floating exchange with formic acid, respectively. (c, d) HRSEM images of formic-acid-treated FePt NC monolayers by free-floating and substrate-supported exchange, respectively.

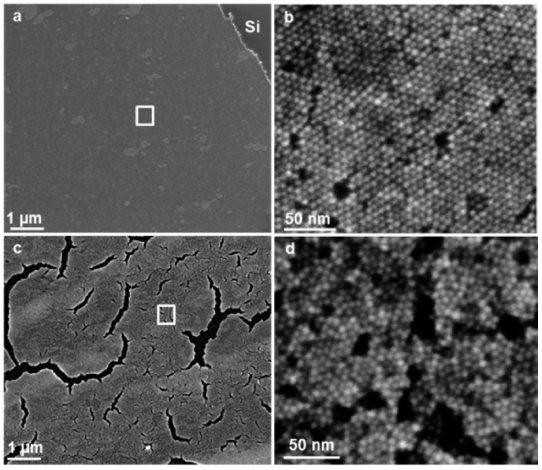

Figure 3. (a, b) SEM images of a thick (four NC layers) FePt NC superlattice film subject to free-floating formic acid exchange followed by secondary substrate-supported exchange: (a) low-magnification SEM image, showing the crack-free film over a large area; (b) HRSEM image of the area indicated in a, showing the well-preserved NC superlattice structure. (c, d) SEM images of a thick (four NC layers) FePt NC superlattice film subject to direct substrate-supported exchange with formic acid: (c) low-magnification SEM image, showing a significant amount of cracks arising from the lost volume; (d) HRSEM image of the area indicated in c, showing the loss of NC ordering.

prior to ligand exchange with formic acid in keeping with previously reported procedures (Figure 2d).[18,19] These findings clearly demonstrate the advantages of this new exchange strategy over previous substrate-supported exchange approaches in maintaining structure integrity of NC superlattice films. Presumably, this is attributed to the high lateral mobility of NCs floating on a liquid surface,[36,37] which enables homogeneous shrinkage of interparticle spacing and therefore macroscopic film contraction during ligand replacement. We note that free-floating treatment alone is not sufficient to achieve complete ligand exchange for thicker NC films (i.e., $\geq$ 4 NC layers), as the short ligands injected may not reach the top NC layers by diffusion through the assembly. To ensure complete removal of the native organic ligands, secondary substrate-supported exchange with formic acid is performed after transferring the formic-acid-treated film to a Si wafer. FTIR confirms the nearly complete removal of organic ligands by this strategy (Figure S1). Interestingly, the film integrity and NC ordering are well-retained upon secondary exchange despite a small amount of voids observed at high magnification (Figure 3a and b). In comparison, direct substrate-supported exchange leads to severely cracked films without NC ordering (Figure 3c and d), similar to the case of monolayers (Figure 2d). These results demonstrate the possibility to obtain continuous and strongly coupled thick NC superlattice films by this two-step exchange approach, which are expected to be highly desirable for applications requiring out-of-plane electrical transport such as solar cells.[38]

Grazing incidence small-angle X-ray scattering (GISAXS) is employed to evaluate NC ordering across large areas and to quantify the change in interparticle spacing before and after ligand exchange.[18] Similar to the pristine FePt NC superlattice film (Figure 4a), the sharp scattering pattern exhibited by the formic-acid-treated film confirms long-range NC ordering over large areas (Figure 4b), whereas the line cuts along the q_y axis of the GISAXS patterns reveal that the exchange process reduces the average in-plane center-to-center distance between neighboring NCs by 2.3 nm to only 0.3 nm (Figure 4d). By contrast, when the same NC film is subject to substrate-supported exchange, the GISAXS pattern lacks evidence of long-range NC ordering (Figure 4c) and exhibits a broadened peak (Figure 4d). This broadening reflects nonuniform interparticle spacing, consistent with the disordered NC assembly structure observed by electron microscopies (Figure 2d).

In addition to FePt NCs, a similar macroscopic film contraction is also observed when Au (3.5 nm)[39] and PbS (9.3 nm)[40] NC films are subject to free-floating exchange with EDT[17] and ammonium thiocyanate (NH_4SCN),[24] respectively (Figure 5a and b), suggesting this approach is applicable to different NCs and short ligands. In both cases, FTIR confirms the removal of the native organic ligands (Figure S2), while TEM and HRSEM establish the preserved long-range NC ordering (Figure 5 and S3). The average interparticle distance is reduced to 0.3 and 0.2 nm for Au and PbS NC films, respectively, as determined by GISAXS and TEM (Figure S4). It is worth noting that the optical properties of Au NC films are drastically affected by the reduced interparticle distance, as evidenced by the apparent color change associated with film contraction (Figure 5a). The purple to gray color change is indicative of enhanced plasmonic coupling of Au NCs, which is also confirmed by the pronounced red-shift of the plasmon band in

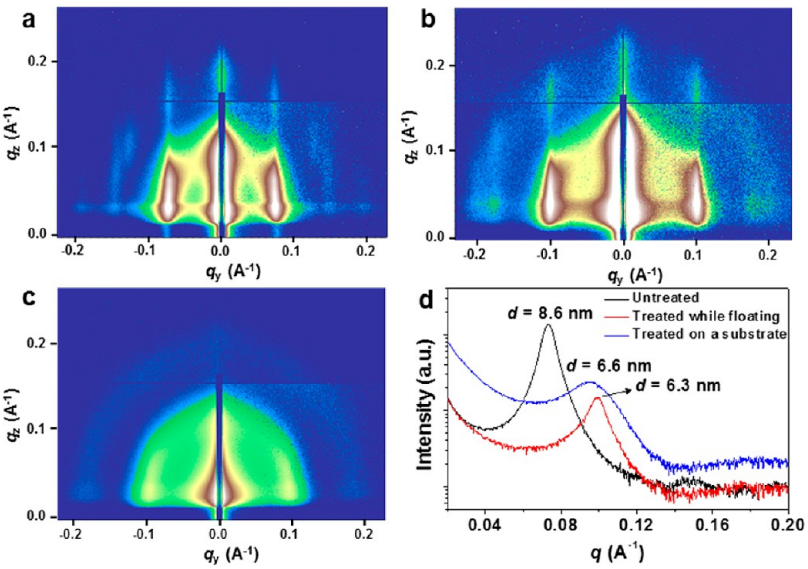

Figure 4. GISAXS patterns obtained from an untreated FePt NC film (a) and formic-acid-treated NC films by free-floating (b) and substrate-supported (c) exchange, respectively. (d) Respective line cuts along the horizontal (q_y) axis, where the center-to-center distance can be calculated from the peak position.

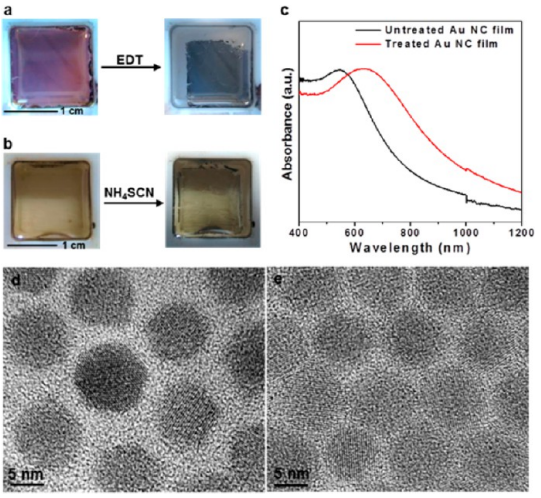

Figure 5. Photographs of Au (a) and PbS (b) NC superlattice films subject to free-floating exchange with EDT and NH_4SCN, respectively. The cracks in the upper right corner of the treated NC films are caused by the syringe. (c) Absorption spectra of Au NC films before and after EDT treatment, respectively. (d, e) HRTEM images of a PbS NC superlattice monolayer before and after free-floating exchange with NH_4SCN, respectively, showing the preserved NC ordering despite the significantly reduced interparticle spacing.

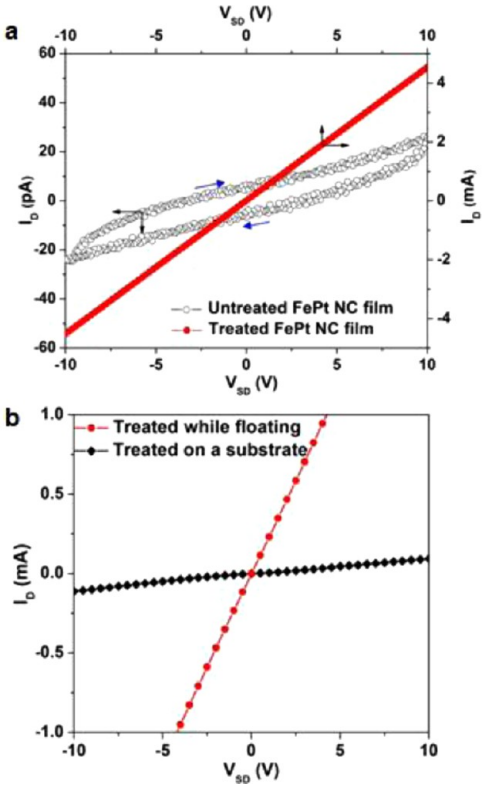

Figure 6. (a) Typical *I*–*V* curves of FePt NC superlattice monolayers before and after free-floating exchange with formic acid, respectively. The blue arrows indicate the voltage scan direction. (b) Typical *I*–*V* curves of formic-acid-treated FePt NC films by free-floating and substrate-supported exchange, respectively.

absorption spectra (Figure 5c). The change of dielectric environment surrounding each NC is also expected to contribute to the observed red shift. Fafarman *et al.* have systematically studied the optical properties of Au NC films treated by EDT and NH_4SCN by using ellipsometric, transmittance, and reflectance spectroscopy as well as numerical simulations.[41] However, to our knowledge, theoretical calculations that can quantitatively determine the contributions of changes to the dielectric environment, bound ligand molecules, and interparticle coupling to the observed color change are still lacking in the literature.

The significant reduction in interparticle spacing decreases the charge tunneling barrier width between

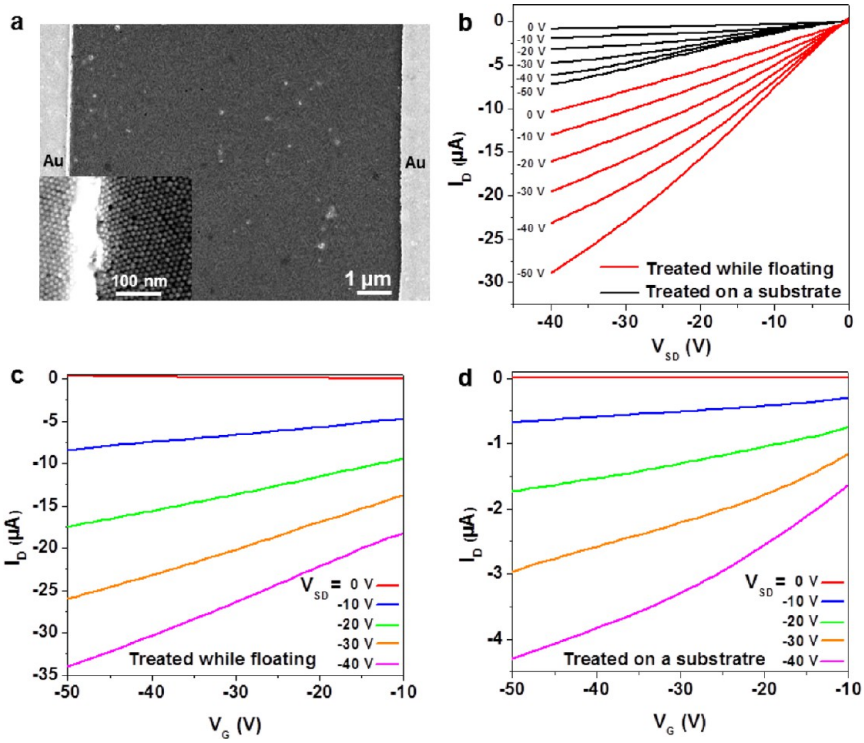

Figure 7. (a) SEM images of a typical FET built from a formic-acid-treated PbS NC monolayer by free-floating exchange. Channel dimensions: length = 10 μm; width = 2000 μm. The inset is a HRSEM image, showing the preserved NC superlattice structure. (b) Output curves of formic-acid-treated PbS NC monolayers by free-floating (red curves) and substrate-supported (black curves) exchange, respectively. (c, d) Transfer curves of formic-acid-treated PbS NC monolayers by free-floating and substrate-supported exchange, respectively.

neighboring NCs, which is expected to facilitate charge transport through NC arrays.[5] To measure electrical properties, the floating NC films are simply transferred to sapphire substrates with prepatterned Au electrodes without further heat treatment. Representative current−voltage (I−V) curves of FePt NC films before and after formic acid treatment are shown in Figure 6a. As expected, the pristine NC superlattice film is essentially insulating due to the large interparticle spacing, whereas free-floating exchange leads to an increase in film conductance by 8 orders of magnitude, with electrical conductivities approaching 3 ± 1 S cm^{-1} (Figure 6a). Note that substrate-supported exchange with formic acid also leads to conductive FePt NC films; however the conductivity obtained is 25-fold lower than that of the film treated while floating (Figure 6b). This result is not surprising considering the significant amount of structural defects resulted from substrate-supported treatment (Figure 2d). In case of Au NCs, free-floating exchange with EDT yields strongly coupled superlattice films with conductivities in the range of 10−90 S cm^{-1}, representing about 7 orders of magnitude enhancement compared with the pristine films consisting of oleylamine-capped Au NCs (Figure S5). We note that the conductivity reported in this work is about 1 order of magnitude higher than that obtained previously for the EDT-treated Au NC films (~2−10 S cm^{-1}),[41] which could be attributed to the different film morphology (film continuity, NC size, and NC ordering, *etc.*) and completeness of ligand-exchange in two experiments.

Thin films of strongly coupled semiconductor NC superlattices are ideal candidates for electronic and optoelectronic devices.[5] We demonstrate this by fabricating field-effect transistors (FETs) by integrating formic-acid-treated PbS NC superlattice films onto Si/SiO_2 substrates with prepatterned Ti/Au source and drain electrodes, with the current flow (I_D) between two electrodes modulated by the application of a gate voltage (V_G). Figure 7a shows SEM images of a FET constructed from a monolayer of PbS NCs, showing that the crack-free superlattice layer covers the entire FET channel. The output curves in Figure 7b reveal *p*-type transport (red curves), consistent with previous results obtained from formic-acid-treated thick PbS NC films made by layer-by-layer dip coating.[21] The hole mobility calculated from the slopes of I_D−V_G plots in the linear regime is 2.7 ± 0.6 × 10^{-3} cm^2 V^{-1} s^{-1} (Figure 7c), 1 order of magnitude greater than that of the FET built from the formic-acid-treated PbS NC monolayer by substrate-supported exchange, which is 2.2 ± 0.7 × 10^{-4} cm^2 V^{-1} s^{-1} (Figure 7d). The lower carrier mobility of the latter case is ascribed to structural defects such as cracks and voids generated during substrate-supported exchange (Figure S6). We note that the formic-acid-treated PbS NC FETs are difficult to turn off, which appears to be consistent with the

results reported previously.[21] We speculate that this could be related to the peculiar surface chemistry (or electronic structure) of PbS NCs induced by formic acid. Further work needs to be done in order to elucidate the underlying physics.

CONCLUSIONS

In summary, we have developed a simple yet efficient ligand-exchange approach to obtain crack-free, strongly coupled NC superlattice films that are not readily accessible by previous exchange methods. The process involves *in situ* chemical treatment of free-floating NC superlattice films preassembled at the liquid−air interface using various short ligands. The high lateral mobility of floating NCs allows macroscopic film contraction with ligand exchange, thus largely preventing film cracking while preserving NC ordering, which in turn significantly improves electrical transport properties of NC films. Moreover, the ready integration of strongly coupled NC superlattice films onto arbitrary substrates offered by our approach paves the way for the development of flexible, high-performance NC-based devices. We note that the improved charge transport in our work may be mainly ascribed to the film continuity rather than the preserved NC ordering, but it will be very interesting to investigate the effect of superlattice ordering on charge transport in the future work. We should also remark that NC surface chemistry may alter the electronic structure of NCs, that is, different short ligands used for exchange could dramatically influence charge transport characteristics of NC films. Therefore, systematic optimization of the NC/short ligand combination to obtain desirable carrier type and mobility is critical to achieving high-performance electronic and optoelectronic devices.

METHODS

Synthesis and Purification of Colloidal NCs. Monodisperse FePt,[35] Au,[39] and PbS[40] NCs, stabilized by oleic acid and/or oleylamine, are synthesized according to literature methods. The as-synthesized NCs are washed twice by centrifugation with ethanol and then are dissolved in hexane to form stable dispersions with concentrations ranging from 1 to 10 mg/mL.

***In Situ* Ligand Exchange of NC Superlattice Films at the Liquid−Air Interface.** Large-area NC superlattice films were obtained by controlled drying a NC solution in hexane on the surface acetonitrile confined in a Teflon well (~1.5 × 1.5 × 1.5 cm^3), following the procedure we reported previously.[34] The film thickness is tunable from monolayers to multiplayers by changing the NC concentration. For *in situ*, free-floating ligand exchange, an acetonitrile solution containing the chosen short ligands (e.g., formic acid, EDT, or ammonium thiocyanate) was slowly injected into the subphase by a syringe at one of the well corners to minimize the damage of the floating NC film. The amount of short ligands injected is determined by their final concentration in acetonitrile subphase, which is typically 20−40 mM for formic acid, 10−20 mM for EDT, and 15−30 mM for NH_4SCN, respectively. Subsequently, the Teflon well was covered by a glass slide for surface treatment, the occurrence of which is manifested by the macroscopic film contraction. After ~30 min of treatment, the floating NC film was transferred to a substrate (Si wafer, TEM grid, or quartz substrate, *etc.*) and rinsed with acetonitrile to remove excess short ligands. For thick NC superlattice films (i.e., ≥ 4 NC layers), secondary substrate-supported exchange was performed to ensure the complete removal of the native organic ligands, following the procedure described previously.[18] To avoid oxidation of NC surface, both self-assembly and ligand exchange processes were performed in a N_2-filled glovebox.

Instrumentation. The liquid-supported NC films were transferred to SiO_2/Si wafers for SEM and HRSEM characterizations, which were carried out on a Zeiss Gemini Ultra-55 microscope operating at 5 kV. For TEM characterization, the floating films were collected on carbon-coated TEM grids, and TEM images were recorded on a JEOL-2100 microscope operating at 200 kV. NC films were transferred to double-side-polished silicon substrates for FTIR measurements, which were carried out on a Perkin-Elmer Spectrum One Spectrometer at a spectral resolution of 4 cm^{-1}. GISAXS measurements were performed at beamline 7.3.3 at the Advanced Light Source, Lawrence Berkeley National Laboratory, using an approximately 0.5 mm wide 10 keV X-ray beam. The image processing was done using the SAS 2D program in Igor Pro. Samples of GISAXS measurements were deposited onto Si wafers. Absorbance spectra of NC films transferred to quartz substrates were recorded on a Varian Cary 5000 UV/vis/NIR spectrophotometer equipped with an integrating sphere.

Electrical Transport Measurements. Samples for electrical conductivity measurements were prepared by transferring the floating NC films to sapphire substrates prepatterned with Au electrodes (two- or four-probe measurements), which were deposited by thermal evaporation through a shadow mask, with a channel length (L) and width (W) of 100 and 3200 μm, respectively. FETs were fabricated by transferring formic-acid-treated PbS NC films onto n-doped Si wafers with 200 nm thermally grown SiO_2, which served as the gate and gate dielectric, respectively. Source and drain Ti/Au (2 nm/38 nm) electrodes were prepatterned onto the SiO_2 surface by thermal evaporation through a shadow mask, with channel length (L) and width (W) of 10 and 2000 μm, respectively. The field-effect carrier mobility (μ_{lin}) was calculated from transfer curves in the linear regime by the equation:[18]

$$\frac{\partial I_D}{\partial V_G}(V_{SD} = \text{constant}) = \frac{WC_iV_{SD}}{L}\mu_{lin}$$

where C_i is the capacitance per unit area of the dielectric layer, W is the channel width, and L is the channel length. All electrical measurements were performed using Agilent 4155C semiconductor parameter analyzer under dry nitrogen atmosphere. The reported electrical conductivities and carrier mobilities are the averages of four devices.

Conflict of Interest: The authors declare no competing financial interest.

Acknowledgment. Work was performed at the Molecular Foundry, Lawrence Berkeley National Laboratory and was supported by the U.S. Department of Energy (DOE) under contract no. DE-AC02-05CH11231. D.J.M. was supported by a DOE Early Career Research Program grant under the same contract. We gratefully acknowledge R. Wang, Y. Zhang, and B. Ma for assistance with FET measurements, Ellen Briggs for PbS NC synthesis, and A. Llordes, E. Chan, and A. Hexemer for assistance with GISAXS, which was carried out at Advanced Light Source (ALS) beamline 7.3.3. A.D. acknowledges startup support from Fudan University, Natural National Science Foundation of China (21373052), and the 973 Program (2013CB934101, 2014CB845602).

Supporting Information Available: Additional FTIR spectra, SEM and TEM images, GISAXS patterns, and $I-V$ curves. This material is available free of charge *via* the Internet at http://pubs.acs.org.

REFERENCES AND NOTES

1. Collier, C. P.; Vossmeyer, T.; Heath, J. R. Nanocrystal Superlattices. *Annu. Rev. Phys. Chem.* **1998**, *49*, 371–404.
2. Tang, Z. Y.; Zhang, Z. L.; Wang, Y.; Glotzer, S. C.; Kotov, N. A. Self-Assembly of CdTe Nanocrystals into Free-Floating Sheets. *Science* **2006**, *314*, 274–278.
3. Murray, C. B.; Kagan, C. R.; Bawendi, M. G. Synthesis and Characterization of Monodisperse Nanocrystals and Close-Packed Nanocrystal Assemblies. *Annu. Rev. Mater. Sci.* **2000**, *30*, 545–610.
4. Tran, T. B.; Beloborodov, I. S.; Lin, X. M.; Bigioni, T. P.; Vinokur, V. M.; Jaeger, H. M. Multiple Cotunneling in Large Quantum Dot Arrays. *Phys. Rev. Lett.* **2005**, *95*, 076806.
5. Talapin, D. V.; Lee, J.-S.; Kovalenko, M. V.; Shevchenko, E. V. Prospects of Colloidal Nanocrystals for Electronic and Optoelectronic Applications. *Chem. Rev.* **2010**, *110*, 389–458.
6. Dong, A.; Chen, J.; Patrick, M. V.; Kikkawa, J. M.; Murray, C. B. Binary Nanocrystal Superlattice Membranes Self-assembled at the Liquid−Air Interface. *Nature* **2010**, *466*, 474–477.
7. Choi, J.-H.; Fafarman, A. T.; Oh, S. J.; Ko, D.-K.; Kim, D. K.; Diroll, B. T.; Muramoto, S.; Gillen, J. G.; Murray, C. B.; Kagan, C. R. Bandlike Transport in Strongly Coupled and Doped Quantum Dot Solids: A Route to High-Performance Thin-Film Electronics. *Nano Lett.* **2012**, *12*, 2631–2638.
8. Sun, L.; Choi, J. J.; Stachnik, D.; Bartnik, A. C.; Hyun, B.-R.; Malliaras, G. G.; Hanrath, T.; Wise, F. W. Bright Infrared Quantum-Dot Light-Emitting Diodes through Inter-dot Spacing Control. *Nat. Nanotechnol.* **2012**, *7*, 369–373.
9. Schliehe, C.; Juarez, B. H.; Pelletier, M.; Jander, S.; Greshnykh, D.; Nagel, M.; Meyer, A.; Foerster, S.; Kornowski, A.; Klinke, C.; *et.al.* Ultrathin PbS Sheets by Two-Dimensional Oriented Attachment. *Science* **2010**, *329*, 550–553.
10. Singh, A.; Dickinson, C.; Ryan, K. M. Insight into the 3D Architecture and Quasicrystal Symmetry of Multilayer Nanorod Assemblies from Moire Interference Patterns. *ACS Nano* **2012**, *6*, 3339–3345.
11. Bodnarchuk, M. I.; Kovalenko, M. V.; Pichler, S.; Fritz-Popovski, G.; Hesser, G.; Heiss, W. Large-Area Ordered Superlattices from Magnetic Wüstite/Cobalt Ferrite Core/Shell Nanocrystals by Doctor Blade Casting. *ACS Nano* **2010**, *4*, 423–431.
12. Evers, W. H.; Goris, B.; Bals, S.; Casavola, M.; Graaf, J.; de Roij, R.; van Dijkstra, M.; Vanmaekelbergh, D. Low-Dimensional Semiconductor Superlattices Formed by Geometric Control over Nanocrystal Attachment. *Nano Lett.* **2013**, *13*, 2317–2323.
13. Panthani, M. G.; Korgel, B. A. Nanocrystals for Electronics. *Annu. Rev. Chem. Biomol. Eng.* **2012**, *3*, 287–311.
14. Pileni, M. P. Self-Assembly of Inorganic Nanocrystals: Fabrication and Collective Intrinsic Properties. *Acc. Chem. Res.* **2007**, *40*, 685–693.
15. Collier, C. P.; Henrichs, S.; Shiang, J. J.; Saykally, R. J.; Heath, J. R. Reversible Tuning of Silver Quantum Dot Monolayers Through the Metal-Insulator Transition. *Science* **1997**, *277*, 1978–1980.
16. Talapin, D. V.; Murray, C. B. PbSe Nanocrystal Solids for n- and p-Channel Thin Film Field-Effect Transistors. *Science* **2005**, *310*, 86–89.
17. Luther, J. M.; Law, M.; Song, Q.; Perkins, C. L.; Beard, M. C.; Nozik, A. J. Structural, Optical and Electrical Properties of Self-Assembled Films of PbSe Nanocrystals Treated with 1,2-Ethanedithiol. *ACS Nano* **2008**, *2*, 271–280.
18. Tangirala, R.; Baker, J. L.; Alivisatos, A. P.; Milliron, D. J. Modular Inorganic Nanocomposites by Conversion of Nanocrystal Superlattices. *Angew. Chem., Int. Ed.* **2010**, *49*, 2878–2882.
19. Choi, J. H.; Luria, J.; Hyun, B.-R.; Bartnik, A. C.; Sun, L.; Lim, Y.-F.; Marohn, J. A.; Wise, F. W.; Hanrath, T. Photogenerated Exciton Dissociation in Highly Coupled Lead Salt Nanocrystal Assemblies. *Nano Lett.* **2010**, *10*, 1805–1811.
20. Baumgardner, W. J.; Whitham, K.; Hanrath, T. Confined-but-Connected Quantum Solids *via* Controlled Ligand Displacement. *Nano Lett.* **2013**, *13*, 3225–3231.
21. Zarghami, M. H.; Liu, Y.; Gibbs, M.; Gebremichael, E.; Webster, C.; Law, M. p-Type PbSe and PbS Quantum Dot Solids Prepared with Short-Chain Acids and Diacids. *ACS Nano* **2010**, *4*, 2475–2485.
22. Zhang, H.; Hu, B.; Sun, L.; Hovden, R.; Wise, F. W.; Muller, D. A.; Robinson, R. D. Surfactant Ligand Removal and Rational Fabrication of Inorganically. Connected Quantum Dots. *Nano Lett.* **2011**, *11*, 5356–5361.
23. Liu, Y.; Gibbs, M.; Puthussery, J.; Gaik, S.; Ihly, R.; Hillhouse, H. W.; Law, M. Dependence of Carrier Mobility on Nanocrystal Size and Ligand Length in PbSe Nanocrystal Solids. *Nano Lett.* **2010**, *10*, 1960–1969.
24. Fafarman, A. T.; Koh, W.-K.; Diroll, B. T.; Kim, D. K.; Ko, D.-K.; Oh, S. J.; Ye, X.; Doan-Nguyen, V.; Crump, M. R.; Reifsnyder, D. C.; *et.al.* Thiocyanate-Capped Nanocrystal Colloids: Vibrational Reporter of Surface Chemistry and Solution-Based Route to Enhanced Coupling in Nanocrystal Solids. *J. Am. Chem. Soc.* **2011**, *133*, 15753–15761.
25. Rosen, E. L.; Buonsanti, R.; Llordes, A.; Sawvel, A. M.; Milliron, D. J.; Helms, B. A. Exceptionally Mild Reactive Stripping of Native Ligands from Nanocrystal Surfaces by Using Meerwein's Salt. *Angew. Chem., Int. Ed.* **2012**, *51*, 684–689.
26. Konstantatos, G.; Howard, I.; Fischer, A.; Hoogland, S.; Clifford, J.; Klem, E.; Levina, L.; Sargent, E. H. Ultrasensitive Solution-Cast Quantum Dot Photodetectors. *Nature* **2006**, *442*, 180–183.
27. Kovalenko, M. V.; Scheele, M.; Talapin, D. V. Colloidal Nanocrystals with Molecular Metal Chalcogenide Surface Ligands. *Science* **2009**, *324*, 1417–1420.
28. Dong, A.; Ye, X.; Chen, J.; Kang, Y.; Gordon, T.; Kikkawa, J. M.; Murray, C. B. A Generalized Ligand-Exchange Strategy Enabling Sequential Surface Functionalization of Colloidal Nanocrystals. *J. Am. Chem. Soc.* **2011**, *133*, 998–1006.
29. Nag, A.; Kovalenko, M. V.; Lee, J.-S.; Liu, W.; Spokoyny, B.; Talapin, D. V. Metal-free Inorganic Ligands for Colloidal Nanocrystals: S^{2-}, HS^{-}, Se^{2-}, HSe^{-}, Te^{2-}, HTe^{-}, TeS_3^{2-}, OH^{-}, and NH_2^{-} as Surface Ligands. *J. Am. Chem. Soc.* **2011**, *133*, 10612–10620.
30. Webber, D. H.; Brutchey, R. L. Ligand Exchange on Colloidal CdSe Nanocrystals Using Thermally Labile *tert*-Butylthiol for Improved Photocurrent in Nanocrystal Films. *J. Am. Chem. Soc.* **2012**, *134*, 1085–1092.
31. Lee, J.-S.; Kovalenko, M. V.; Huang, J.; Chung, D. S.; Talapin, D. V. Band-like Transport, High Electron Mobility and High Photoconductivity in All-inorganic Nanocrystal Arrays. *Nat. Nanotechnol.* **2011**, *6*, 348–352.
32. Kim, D. K.; Lai, Y.; Diroll, B. T.; Murray, C. B.; Kagan, C. R. Flexible and Low-Voltage Integrated Circuits Constructed from High-Performance Nanocrystal Transistors. *Nat. Commun.* **2012**, *3*, 1216.
33. Sargent, E. H. Colloidal Quantum Dot Solar Cells. *Nat. Photonics* **2012**, *6*, 133–135.
34. Dong, A.; Chen, J.; Oh, S. J.; Koh, W.; Xiu, F.; Ye, X.; Ko, D.; Wang, K. L.; Kagan, C. R.; Murray, C. B. Multiscale Periodic Assembly of Striped Nanocrystal Superlattice Films on a Liquid Surface. *Nano Lett.* **2011**, *11*, 841–846.
35. Sun, S.; Murray, C. B.; Weller, D.; Folks, L.; Moser, A. Monodisperse FePt Nanoparticles and Ferromagnetic FePt Nanocrystal Superlattices. *Science* **2000**, *287*, 1989–1992.
36. Isa, L.; Kumar, K.; Muller, M.; Grolig, J.; Textor, M.; Reimhult, E. Particle Lithography from Colloidal Self-Assembly at Liquid−Liquid Interfaces. *ACS Nano* **2010**, *4*, 5665–5670.
37. Pradhan, S.; Xu, L. P.; Chen, S. W. Janus Nanoparticles by Interfacial Engineering. *Adv. Funct. Mater.* **2007**, *17*, 2385–2392.
38. Kramer, I. J.; Sargent, E. H. Colloidal Quantum Dot Photovoltaics: A Path Forward. *ACS Nano* **2011**, *5*, 8506–8514.
39. Peng, S.; Lee, Y.; Wang, C.; Yin, H.; Dai, S.; Sun, S. A Facile Synthesis of Monodisperse Au Nanoparticles and Their Catalysis of CO Oxidation. *Nano Res.* **2008**, *1*, 229–234.
40. Joo, J.; Na, H. B.; Yu, T.; Yu, J. H.; Kim, Y. W.; Wu, F.; Zhang, J. Z.; Hyeon, T. Generalized and Facile Synthesis of Semiconducting Metal Sulfide Nanocrystals. *J. Am. Chem. Soc.* **2003**, *125*, 11100–11105.
41. Fafarman, A. T.; Hong, S.-H.; Caglayan, H.; Ye, X.; Diroll, B. T.; Paik, T.; Engheta, N.; Murray, C. B.; Kagan, C. R. Chemically Tailored Dielectric-to-Metal Transition for the Design of Metamaterials from Nanoimprinted Colloidal Nanocrystals. *Nano Lett.* **2013**, *13*, 350–357.